

DESIGN AND SIMULATION OF MEMBRANE SUPPORTED TRANSMISSION LINES FOR INTERCONNECTS IN A MM-WAVE MULTICHIP MODULE

N. E. S. Farrington

e2v Technologies
Carholme Rd, Lincoln, LN1 1SF, UK

S. Iezekiel

Department of Electrical and Computer Engineering
University of Cyprus, Cyprus

Abstract—Investigations are conducted into low-loss, low-dispersion fully shielded membrane-supported striplines designed for use in a millimeter-wave multi-chip-module. Two types of transmission line are studied: a membrane-supported shielded stripline and a novel variation of this where the membrane material is removed in areas of little mechanical importance to reduce attenuation and dispersion. The latter is possible through the exploitation of a versatile micromachining technique using SU-8 for both the membrane and the shielding. The micromachining techniques used for the fabrication of the micro-shielding allows for the conformal packaging of lines and devices, with the ultimate aim of the realization of novel components for 3D system-in-a-package type modules. Extensive simulated results obtained from rigorous electromagnetic modeling are presented that fully characterize both types of line and, where possible, are compared to measured results. Loss mechanisms are investigated for both line types and simulations suggest that losses as low as 0.39 dB/cm and effective relative permittivities of less than 1.05 are possible at a frequency of 100 GHz, comparing well with other demonstrated membrane supported transmission lines. The methods used for investigation of line characteristics and analysis of single-mode, non-leaky frequency range are applicable to any variety of membrane supported transmission line. The basics of line fabrication are given along with measurement results and de-embedding techniques used at V-band.

1. INTRODUCTION

The advantages of membrane-supported lines and passive components for millimeter-wave frequencies include extremely low-loss and dispersion along with the potential for high-performance passives such as inductors, capacitors [1], directional couplers [2] and antenna arrays [3]. In addition the fabrication of thin-film passive components directly onto a membrane has been demonstrated [2]. Although extremely thin ($\sim 1.5 \mu\text{m}$), the $\text{SiO}_2/\text{Si}_3\text{N}_4/\text{SiO}_2$ membranes demonstrated (and low mass membranes in general) are relatively strong as gravitational forces scale with mass³ [4], and have reportedly survived NASA's space launch vibration tests after the epoxy attachment of planar Schottky diodes [5] (for a membrane area of 0.5 cm^2).

The work on novel micromachined quasi-planar transmission line interconnects has mostly been based on silicon substrates. This is due to a combination of the excellent mechanical and micromachining properties of silicon [6] and maturity of the associated processing techniques [7]. In addition, the use of silicon allows for application of the lines to the rapidly advancing field of RF MEMS [8, 9], which is also predominantly based on silicon technologies. These lines generally revolve around the fabrication of micro-shielding, and the use of a membrane or other methods of removing dielectric material from regions in which the electric field is concentrated [10, 11]: these concepts are illustrated in the lines shown in Figure 1.

The removal of dielectric in which the electric field would otherwise concentrate reduces both the loss and dispersion of the line. However, it is theoretically known and experimentally demonstrated [12] that the inclusion of shielding, although suppressing interference effects and radiation losses from the line, can increase ohmic loss compared to an unshielded line. This means the design of micromachined, shielded transmission lines requires consideration of the ultimate application and operational environment along with careful investigation and optimization of line characteristics.

Demonstrated state-of-the-art performance for micromachined transmission lines includes loss levels of 1.9 dB/cm and 1.25 dB/cm respectively for the elevated and overlay co-planar waveguide (CPW) lines shown in Figures 1(a) and (b) respectively (in comparison to 2.65 dB/cm for a similar conventional CPW) [13]. The reduced dielectric CPW line shown in Figure 1(c) demonstrated a loss of 1.18 dB/cm and effective permittivity of 2.7 at 60 GHz [14] (reduced from 1.64 and 5.6 respectively), while the shielded microstrip lines in Figures 1(e) and (f) exhibited losses of 0.8 dB/cm and 1.9 dB/cm

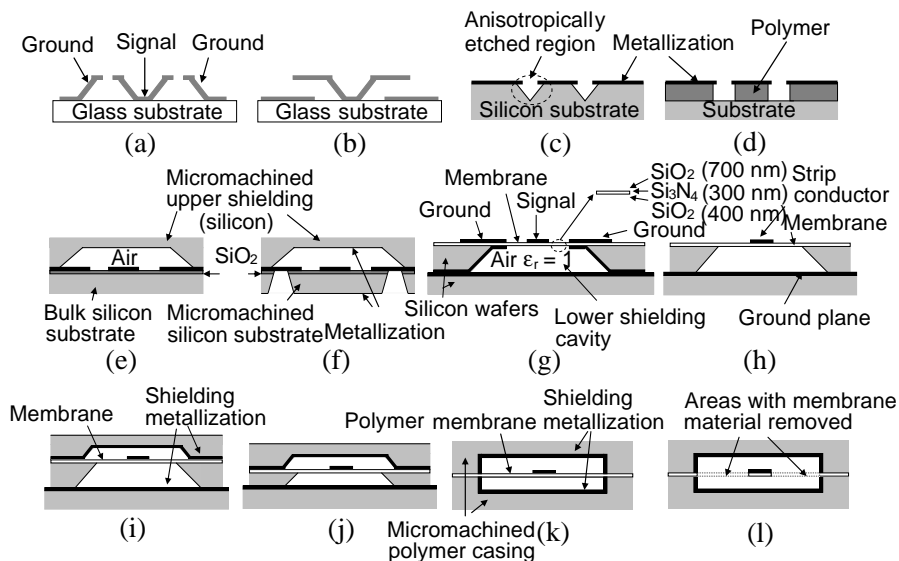


Figure 1. Demonstrated micromachined transmission lines for use at millimeter-wave frequencies: (a) and (b) CPW geometries using raised conductors [13], (c) and (d) CPW using bulk micromachining to remove dielectric in the areas of electric field concentration [14–16], (e) and (f) CPW with micromachined shielding [12], (g) membrane supported CPW (microshield) [17], [7] (h) membrane supported microstrip [3], (i) membrane supported, partially shielded microstrip [3], (j) membrane supported partially shielded stripline [3], and (k) and (l) the fully shielded membrane supported striplines investigated in this paper.

respectively at 40 GHz [12], and thus illustrated the additional ohmic loss introduced through the incorporation of extra shielding. The ‘microshield’ line shown in Figure 1(g) demonstrated a loss of around 0.6 dB/cm at 60 GHz [17] and an effective relative permittivity of 1.08 across W-band [7]. The shielded membrane supported microstrip line illustrated in Figure 1(j) has demonstrated a loss of 0.4 dB/cm at 60 GHz rising to around 0.6 dB/cm at 110 GHz, with an effective permittivity of approximately 1.05 [3].

The micromachined shielded interconnects described in this paper (Figures 1(k) and 1(l)) rely on the use of a versatile photo-epoxy, SU-8 [18–22], which has already been proven in micromachining applications, for the fabrication of both the shielding and the membrane. This fabrication method involves the stacking of photolithographically defined layers (between 10 μm and 500 μm) to

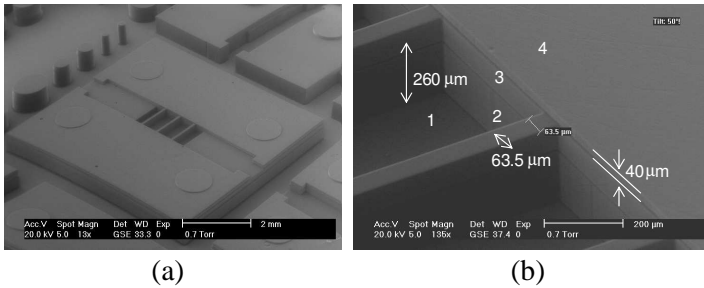


Figure 2. Scanning electron microscope images of complex, multi-layer shielding structures fabricated using SU-8 [22]: (a) Whole structure, (b) close up of ‘ridged’ region.

create complex 3D shielding configurations as shown in Figure 2. For the membrane itself a $10\ \mu\text{m}$ thick layer is applied to a carrier substrate upon which the circuit metallization has already been patterned. The membrane supported circuit can then be lifted off the substrate by dissolving a sacrificial release layer.

Although micromachined silicon platforms have some benefits over polymer and epoxy technologies including process maturity, generally higher chemical resistance and thinner membranes than those achievable using polymers, the level of geometrical complexity of the shielding structures which can be micromachined using polymers and epoxies is higher. This gives increased flexibility and scope which can be exploited to provide a platform with increased versatility. Compared to their silicon counterparts, the SU-8 membranes display increased sturdiness and their processing supports the ability to remove areas of the membrane which are not mechanically important to gain performance advantages.

2. DESIGN AND ELECTROMAGNETIC MODELING

The novel transmission lines consists of a thin dielectric (SU-8) membrane (on which the transmission line metallization is patterned) clamped between two metal coated housing or shielding pieces (also fabricated from SU-8), and is shown schematically in Figure 3. Here it can be seen that the only difference between the two types of line is that regions of the supporting membrane have been removed in one of them (Figure 3(b)). Figure 3(c) illustrates the concept of using supporting beams to ensure the mechanical integrity of the reduced membrane. The successful fabrication of both types of line has been demonstrated using SU-8 and the fabrication techniques are described

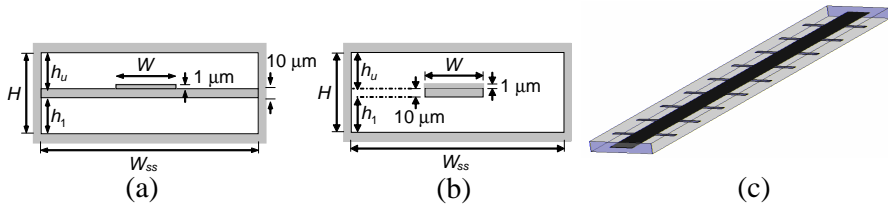


Figure 3. Membrane supported stripline with micromachined conformal shielding, (a) full membrane version, (b) reduced membrane version, and (c) reduced membrane version with supporting beams.

in detail in [22].

When choosing the dimensions of the lines several factors were considered. The thickness of the membrane was kept to a minimum whilst still ensuring structural integrity, so dielectric losses would be reduced as far as possible: this thickness was set at $10\ \mu\text{m}$. In selecting the width and height of the shielding sections, several conflicting factors needed to be considered. In order for the lines to be viable for the intended function (a millimeter-wave MCM), the overall cross-section must be kept to a minimum in both dimensions to achieve a high interconnect density. The cross-section must also be small enough to avoid the propagation of hollow pipe waveguide and surface wave modes in the operational frequency range. However, as the height of the shielding is reduced, the field concentration in the dielectric is increased leading to higher loss and dispersion (this is simulated in Section 2.1). This means that if circumstances permit, the height of the shielding on the opposite side of the membrane to the line metallization should be increased while minimising the height of the opposite shielding, forcing the electric field into an inverted microstrip type configuration and minimising its concentration in the dielectric. The dimensions were chosen such that the total height and width of the shielding were $250\ \mu\text{m}$ and $1\ \text{mm}$ respectively in order to demonstrate a high level of integration. The need for a high integration density also led to the decision to adopt a suspended substrate stripline configuration rather than a suspended inverted microstrip geometry. The position of the metallization was therefore set to be halfway between the upper and lower shielding, meaning the distance between the membrane and the upper shielding, h_u , was $125\ \mu\text{m}$ and the distance from the lower shielding, h_l , was $115\ \mu\text{m}$. The dimensions of the line metallization patterned on the membrane depend on the required electrical characteristics of the line. The metallization thickness was fixed at $1\ \mu\text{m}$ to satisfy skin depth requirements at $50\ \text{GHz}$ (the lowest frequency of interest). The loss tangent of the SU-8

was set as 0.08 to reflect the highest value reported in the literature [22], and the relative permittivity as 3.7.

Due to the quasi-TEM nature of the line, any closed form expressions describing line characteristics tend to be curve-fitted to numerically or experimentally obtained data and so are only valid for certain ranges of geometrical parameters and frequency. An example of this is given in [23] where the expressions have been fitted to simulated data in such a way as to be unusable outside the given geometrical parameter ranges. The thickness of the dielectric membranes used in this work falls outside the usable ranges of all the published closed form expressions found. Instead the commercially available electromagnetic simulation package Ansoft High Frequency Structure Simulator (HFSS) was used [24]. This frequency domain solver was ultimately chosen due to the increased geometrical flexibility it offers when compared to the other solvers available, along with its rigorous electromagnetic solution method. All the simulations described in this paper were performed using stricter solution convergence criteria than the default values (a maximum delta S of 0.01 and two converged passes before final solution) and all frequency sweeps were performed as discrete sweeps: although this is slower than the fast and interpolating sweeps available in HFSS, the solution accuracy is higher.

2.1. Simulation of the Membrane Supported Striplines

The effect of varying the width of the signal conductor on the characteristic impedance and effective permittivity is shown in Figure 4(a) for both types of line. This simulation was performed at 60 GHz using a ports-only solution (all subsequent simulations were performed on a full 3D model using a modal solution). As the strip-width is increased the characteristic impedance decreases due to the increased capacitance and decreased inductance of the structure, which is expected. The effective relative permittivity for the full membrane line is seen to decrease and then increase with increasing strip conductor width for the full membrane line, but not for the reduced membrane line. This effect is due to the current, and therefore electric field becoming increasingly concentrated at the strip conductor edges as frequency increases. At high frequencies, as the strip conductor width is increased, the electric field distribution becomes increasingly concentrated between the strip and sidewall conductors for larger strip conductor widths: in the full membrane line the field is concentrated in the dielectric membrane (thus increasing the effective relative permittivity and dielectric losses of the line), whereas in the reduced membrane line the field is concentrated in air. This is shown in the electric field plots given in Figure 5.

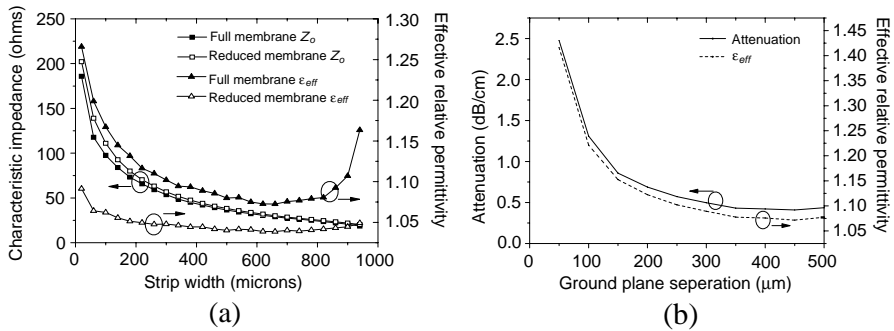


Figure 4. (a) Characteristic impedance and effective relative permittivity variation with strip width for both the full and reduced membrane lines (at 60 GHz), and (b) attenuation characteristic and effective relative permeability variation with increasing ground plane separation for a full membrane line of nominal $50\ \Omega$ impedance at 60 GHz.

It can be seen from Figure 4(a) that a characteristic impedance of $50\ \Omega$ is obtained with a strip-width of $340\ \mu\text{m}$ leading to an effective dielectric constant of around 1.097 for the full membrane lines, and $360\ \mu\text{m}$ with an effective dielectric constant of 1.044 for the reduced membrane line. It is noted at this point that the lower effective permittivity has the effect of slightly increasing the characteristic impedance of the line due to the associated lower capacitance of the structure.

The effect of ground plane separation on the overall loss and effective relative permittivity for a $50\ \Omega$ full membrane line is shown in Figure 4(b). As expected it is seen that the loss and effective relative permittivity decrease as the separation distance is increased due to the lower field concentration in the dielectric membrane.

2.1.1. Simulation of Loss Mechanisms in the Lines

To examine loss mechanisms in the transmission lines, the contributions of the conductor and dielectric loss were simulated separately along with the total loss, all of which are shown in Figure 6 for both line types. Initially the strip conductor and shielding conductivity were set to that of gold with a perfectly smooth surface. In subsequent simulations the effects of an r.m.s. surface roughness of 40 nm on one side of the strip conductor (corresponding to the measured value for the electroplated gold used in line fabrication) and 10 nm on the upper and lower ground planes (corresponding to the

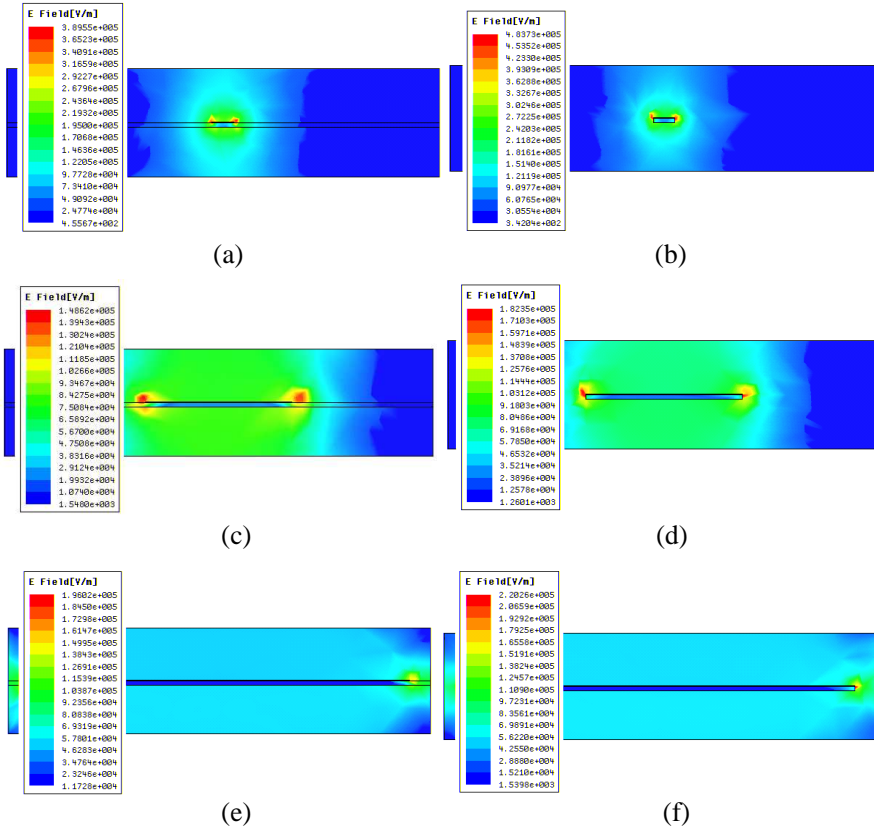


Figure 5. HFSS calculated electric field distributions in membrane supported shielded striplines at 60 GHz for (a) full membrane line with a narrow strip conductor, (b) reduced membrane line with a narrow strip conductor, (c) 50Ω full membrane line, (d) 50Ω reduced membrane line, (e) full membrane line with a wide strip conductor, and (f) reduced membrane line with a wide strip conductor.

measured value for the RF-sputtered gold on the layer's surface) were taken into account.

In the full membrane line the greatest contribution to the loss is that of the conductors until the frequency reaches around 18 GHz. Here it is overtaken by the dielectric loss which increases at a greater rate with frequency. Also, as expected, a slightly greater increase in conductor loss with frequency is seen below 10 GHz where the metal thickness is less than (or significant when compared to) the skin-depth. The total simulated loss is 0.57 dB/cm at 60 GHz, and 0.88 dB/cm at

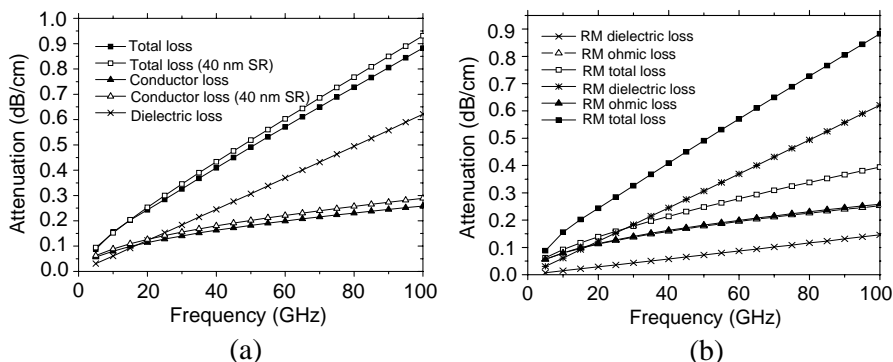


Figure 6. (a) Breakdown of loss mechanisms for a nominally 50 Ω full membrane line, and (b) a comparison of loss contributions in nominally 50 Ω full and reduced membrane lines.

100 GHz which is comparable to the loss values of the state-of-the-art transmission lines previously demonstrated. The inclusion of realistic surface roughness values in the simulations slightly increases the loss to approximately 0.05 dB/cm at 100 GHz.

In the case of the reduced membrane line a drastic reduction is seen in the dielectric-related loss compared to the full membrane version. This is mirrored in the total loss which is around 0.279 dB/cm at 60 GHz and 0.39 dB/cm at 100 GHz. This equates to an improvement of over 50% compared to the full membrane results. The contribution of conductor surface roughness to the loss (not shown) is again an increase of about 0.05 dB/cm at 100 GHz. It is also noted that in the case of the reduced membrane line, the dielectric contribution to the loss is less than that of the conductors throughout the frequency range studied.

2.1.2. Simulation of Line Dispersion Characteristics

The dispersion characteristics of nominally 50 Ω lines over a frequency range of 5 GHz to 100 GHz were then investigated and the results are shown in Figure 7. As expected, a very low dispersion is exhibited by both lines. The full membrane line showed an increase in effective relative permittivity of only 0.00087 over the whole frequency range (around 8/10000 over a decade bandwidth), which is comparable to the measured results for a microshield line given in [52]. The reduced membrane line showed a smaller increase (around half that of the full membrane line) in effective relative permittivity 0.00041 over the same frequency range.

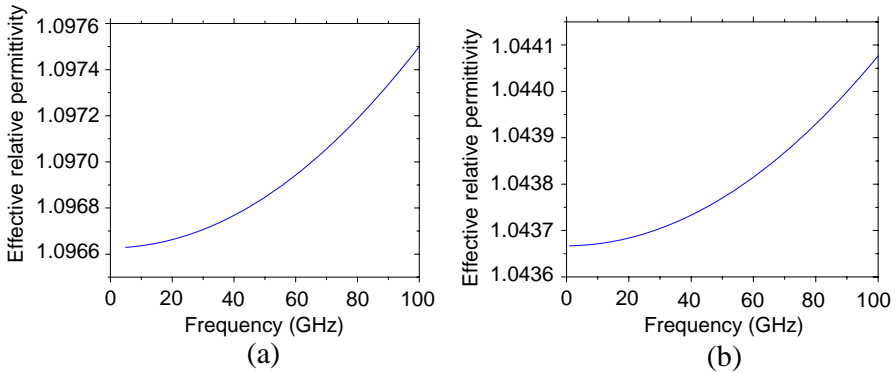


Figure 7. Dispersion characteristics for the membrane-supported shielded striplines with a nominal impedance of $50\ \Omega$: (a) Full membrane line ($340\ \mu\text{m}$ stripwidth), and (b) reduced membrane line ($360\ \mu\text{m}$ stripwidth).

2.1.3. Simulation of the Effects of Reduced Membrane Strip Support Beams

A potential issue with the reduced membrane line is that of mechanical stability. Although the forces on the strip conductor and its supporting beam would be extremely low, the possibility of the beam sagging in the middle, especially under elevated temperatures, may need addressing. A solution to this potential problem would be the addition of supporting beams connecting the supporting membrane to the sidewalls as shown Figure 3(c).

Besides increasing attenuation on the line, the supporting beams can potentially form a periodic structure along the length of the line. To investigate the effects of adding side supports to the line the 3D HFSS model was modified to include $10\ \mu\text{m}$ thick supporting beams with a width of $100\ \mu\text{m}$ and the period was varied from 2 mm to 0.5 mm (for a line length of 1 cm). A full modal simulation of the HFSS model was performed and the results are shown in Figure 8.

It can clearly be seen that for the configurations studied, no significant filtering effect is present. The ripples on both plots can mostly be attributed to the line under study being an integer multiple of half-wavelengths at the relevant frequencies. Figure 8(b) does however show a shift in the $|S_{11}|$ minima which fall above 60 GHz for the 1 and 2 mm period lines. This slight effect is thought to be due to the period of the supports on the respective lines being a half and a quarter of a guided wavelength at the relevant frequencies. Although attenuation (Figure 8(a)) on the line increases as the period of the

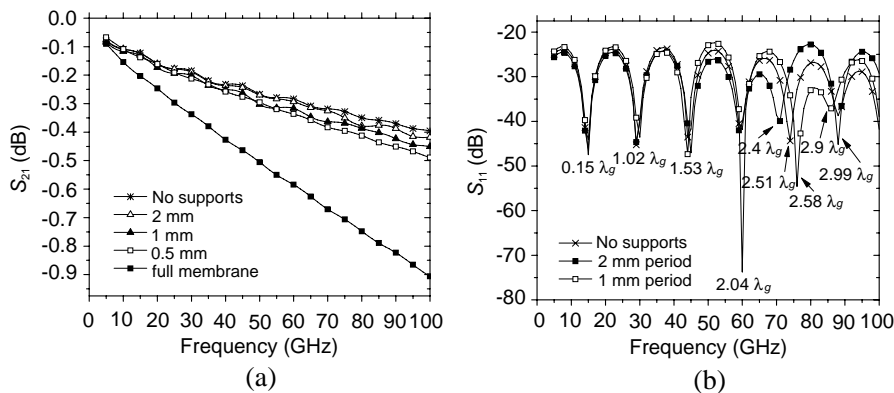


Figure 8. The electrical effects of side support addition a 1 cm long reduced-membrane line: (a) $|S_{21}|$, and (b) $|S_{11}|$ (0.5 mm period and full membrane trace omitted for the sake of clarity).

supports decreases, the loss is at worst almost half that of the full membrane line at 100 GHz.

For the application of this type of line as a MCM interconnect, line lengths of more than a few centimetres are not anticipated. If longer lengths were required, possibly at frequencies higher than those simulated, any filtering effects could be mitigated by introducing a non-periodic configuration of the supporting beams.

3. ANALYSIS OF SINGLE-MODE, NON-LEAKY PERFORMANCE RANGE

Depending on a transmission line’s geometry and operating frequency range, power can be coupled from the dominant (in this case stripline) mode into higher-order and parasitic (or leaky) modes leading to attenuation, increased dispersion and perturbation of the dominant mode’s electric field distribution, thus affecting the desired line characteristics. For the membrane-supported shielded stripline configuration studied, the electric field patterns for the first parasitic and higher-order modes are shown in Figure 9.

All of these modes can be suppressed through correct choice of the shielding parameters for the frequency range of interest [25]. In the case of the parasitic rectangular waveguide TE_{10} mode shown in Figure 9(a), suppression can be achieved by choosing the side shielding separation such that,

$$W_{SS} < \frac{c}{2f_{\max}\sqrt{\epsilon_{\text{reff}}}} \tag{1}$$

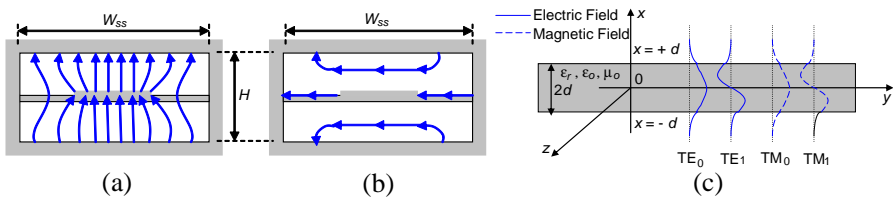


Figure 9. Electric field patterns for (a) parasitic rectangular waveguide TE_{10} type mode, (b) the first higher-order stripline mode (after [25]), and (c) the four lowest propagating modes on a dielectric slab with thickness $2d$: Field intensity is shown as an excursion along the y axis (after [28]).

where f_{\max} is the highest frequency of interest. This sets the maximum side shielding separation to be half a guided-wavelength at the highest frequency. For suppression of the first higher-order stripline mode shown in Figure 8(b), the following restriction must be imposed:

$$H < \frac{c}{4f_{\max}\sqrt{\epsilon_{\text{reff}}}} \quad (2)$$

setting the maximum ground conductor separation to be a quarter of the guided wavelength at the highest frequency of interest. For the structures simulated, Equation (1) gives the highest single-mode frequency of operation as 143 GHz for the full membrane line structure and 146 GHz for the reduced membrane line structure.

As with the enclosed stripline geometry studied, most varieties of quasi-TEM planar transmission line, are susceptible to parasitic (or leaky) modes at certain frequencies [26–30] in addition to higher-order modes. A leaky mode is a guided-wave mode of the background structure into which power can be coupled from the dominant bound mode of the transmission line (the background structure is defined as that of the transmission line with the signal conductor removed or its effects ignored). Although in certain applications this energy leakage can be used to an advantage such as couplers and antennas [28], the effect is generally undesirable leading to increased insertion loss, dispersion, and interference with the bound dominant mode. There are two distinct cases of leakage in planar transmission lines: that effecting slot-based lines and that occurring in both slot and strip-based lines.

In the case of slot-based lines such as CPW and slotline, leakage is usually restricted to higher frequencies where the background modes are usually surface-wave modes, the lower-order of which exhibit a low-frequency cut-off at DC. Here leakage into these modes will only occur above the frequency at which the propagation constant of the

background mode exceeds that of the dominant bound mode [27, 31]. This would have to be considered if a CPW type line was to be implemented.

In the case of quasi-TEM strip-based lines such as microstrip and inhomogeneous stripline (such as those studied here), low-frequency leakage into the background modes can also occur in addition to that at high frequencies [26, 28–32]. In the case of a stripline with a small air gap above the conductor, the background mode takes the form of a parallel-plate waveguide [30] (unless it is fully enclosed leading to a rectangular waveguide geometry as is the case in this work). It has been shown here that in addition to the bound dominant mode, an independent leaky dominant mode exists due to this air gap. The leaky mode is classed as dominant as its current distribution on the strip conductor is similar to that of the TEM mode in homogeneous stripline (as opposed to higher-order modes which display a very different current distribution). This leaky mode is in effect the mechanism by which energy is leaked away from the strip conductor and into the background TM_0 parallel plate mode (whose low-frequency cut-off is at DC).

It has been shown in [33] that with suspended substrate stripline geometries (without side-shielding), the described low-frequency leakage does not occur for most practical geometries. Due to the completely enclosed geometry of the lines considered, the first leaky mode to propagate would be that of a TE_{10} mode (shown in Figure 9) of the inhomogeneously loaded rectangular waveguide formed by the shielding cavity and membrane as opposed to the TM_0 mode of a parallel-plate waveguide. As already calculated using Equation (1), this mode is non-propagating through the frequency range of single-mode stripline propagation since, unlike the parallel-plate TM_0 mode, it has a non-DC low-frequency cut-off.

3.1. Further Discussion of Surface Wave Propagation Characteristics

These modes are typified by a field which decays exponentially away from the dielectric surface with most of the field concentrated near or in the dielectric (Figure 9(c)). The surface-wave modes of propagation are potentially supported due the membrane material acting as a dielectric slab and effectively representing an open boundary waveguide. Surface wave modes of both TM and TE type can be guided along a dielectric slab: in the metallised regions of the membrane, TE_0 and TM_1 mode propagation is not supported (i.e., only even TM and odd TE modes are supported), whereas all modes are supported in the membrane regions with no conductor backing.

For the shielded membrane supported stripline geometries studied here (and stripline geometries in general) the excitation of a surface-wave mode on the dielectric membrane can generally be ruled out. This is due to the presence of upper and lower ground planes which suppresses radiation losses and therefore any surface wave modes. In unshielded membrane configurations employing slot-based lines, surface waves with a DC low-frequency cut-off exist, but with leakage into the dominant surface-wave mode only occurring at frequencies above that where its propagation constant exceeds that of the dominant bound mode [26–29, 31, 35]. However this has not yet proved an issue for this type of line [35] as the propagation constant of a surface wave mode is extremely low for the very thin membranes studied at the frequencies of interest.

In a membrane-supported stripline with no side shielding, a surface wave on the membrane will not propagate until the distance between the strip conductor and the lower shielding becomes electrically large enough to negate the effects of the shielding [30, 32–34]. At this point, the TM_0 parallel plate mode between the strip conductor and shielding begins to act like a TM_0 surface wave bound to the membrane [34]. This is illustrated by the following pairs of simultaneous equations, where Equation (3) describes the case of the TM_0 mode in an inhomogeneously loaded parallel waveguide with uniform cross-section [34], and Equation (4), a TM_0 surface wave [34]. In all the expressions ε_r is that of the dielectric material, d is the thickness of the dielectric material and b represents the distance between the dielectric and the opposite parallel plate conductor. The cutoff wavenumbers are h and k_c in the air and dielectric regions respectively, which can be obtained for each case through the simultaneous solution of the relevant set of equations, and k_o is the free-space wavenumber.

$$\varepsilon_r h \tanh hb = k_c \tan k_c d \quad (3a)$$

$$(\varepsilon_r - 1)k_o^2 = k_c^2 + h^2 \quad (3b)$$

$$\varepsilon_r h = k_c \tan k_c d \quad (4a)$$

$$(\varepsilon_r - 1)k_o^2 = k_c^2 + h^2 \quad (4b)$$

Here it can be seen that for a large frequency and membrane thickness product, the hyperbolic tangent term becomes unity and Equation (3a) reduces to that of (4a) representing the propagation characteristics of an even TM surface wave mode. In our configuration, a parallel plate mode between the strip and ground conductor will not be supported due to the presence of the side shielding. It can therefore be said that a surface wave mode will not exist until the electrical

distance to the ground plane is so large as to have no effect on the field distribution. This would be far outside the range of single mode operation for the lines considered here.

4. HIGH-FREQUENCY MEASUREMENT OF FABRICATED LINES

A selection of test pieces containing various line lengths (500 μm , 1000 μm , and 1844 μm) was fabricated using the micromachining techniques described in [22]: a 3D model of one of the test pieces (a reduced membrane supported shielded line) is shown in Figure 10(a). The supporting membrane was 10 μm thick SU-8 and incorporated passive alignment features, complimentary to those of the shielding block. In addition the membrane featured thickened regions in the vicinity of the probe pads for mechanical strength. The supported line was electroplated with gold to a thickness of 1 μm , while the shielding was sputtered with gold to a thickness of 1 μm . The test pieces were designed to clamp together as shown in Figure 10(a), and micrographs of the membrane (before release from a sacrificial substrate) and wafer probe region of a finished test piece, are shown in Figure 10(b) and Figure 10(c) respectively. Besides test transmission lines, a through, line, reflect (TRL) calibration set was designed and fabricated in order to de-embed the effects of the CPW probe landing pads and transitions from CPW to the shielded membrane supported stripline.

Measurement was performed across a frequency range of 40 GHz to 80 GHz using an Agilent 8510XF coaxial vector network analyser (VNA) and Picoprobe GSG CPW probes. Due to mechanical failure of some of the probing regions during the initial TRL calibration procedure, a full calibration could not be performed. The original motivation for fabricating the probing pads on a region of thickened membrane as opposed to bulk material was to avoid substrate modes which, as documented in [17, 36–40], threaten the repeatability of a TRL calibration.

The remaining lines (500 μm and 1000 μm full-membrane, along with 1000 μm and 1865 μm reduced-membrane lines) were modified to withstand probing. This involved carefully applying quick-setting epoxy at the ends of the lines in the gap between the membrane and the lower shielding and allowing it to be drawn underneath via capillary action until the probe-pad regions were fully supported. Due to the rapidly changing viscosity of the epoxy the distance varied in each instance with the range being measured at between 120 μm and 300 μm .

A calibration was then performed using an impedance standard

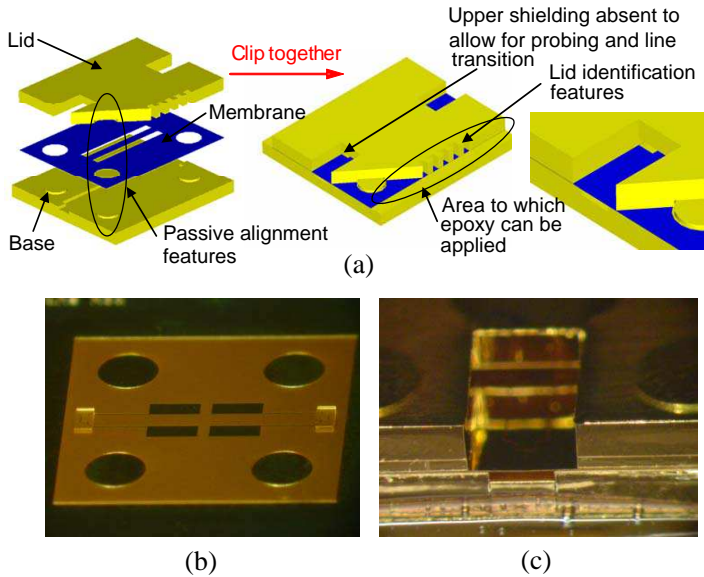


Figure 10. (a) A 3D CAD drawing of a test piece (reflect standard from a TLR calibration set) showing the assembly process including self alignment of the pieces though the use of mechanical alignment features, (b) a micrograph of a membrane supported line before release including detail of the thickened membrane in the vicinity of the CPW probe pads, and (c) the membrane clamped between the two shielding pieces.

substrate (ISS) which set the reference planes for the measurement at the tips of the wafer probes. As these results could not be fully de-embedded, the probe-pads, tapers, and membrane-supported CPW along with the discontinuities between them also contribute to the results. In addition, the introduction of epoxy underneath the membranes in the probe-pad and GCPW (CPW with epoxy underfill) regions will have altered the electrical characteristics away from their designed values.

To investigate the effects of this on the measured data, a simplified model of the measured lines (Figure 11(a)) was created in Microwave Office [41] using a cascade of lines representing the different regions of those tested. Sections of ideal transmission line with the same physical length as those in the measured structures were used, and the electrical characteristics calculated using HFSS. The electrical properties of the epoxy under-fill were taken to be those of SU-8 (itself an epoxy) leading to the approximate values listed in Figure 11(b).

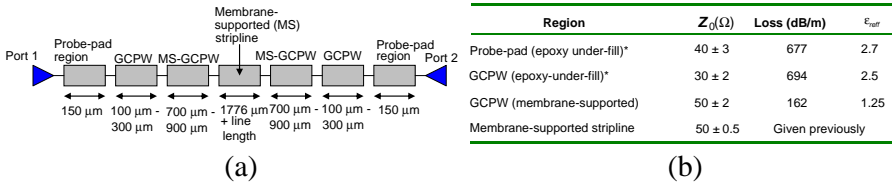


Figure 11. (a) Simplified model of the measured lines used for Microwave Office® simulations, and (b) electrical characteristics of cascaded line sections simulated using HFSS™ at 60 GHz (* denotes estimated values).

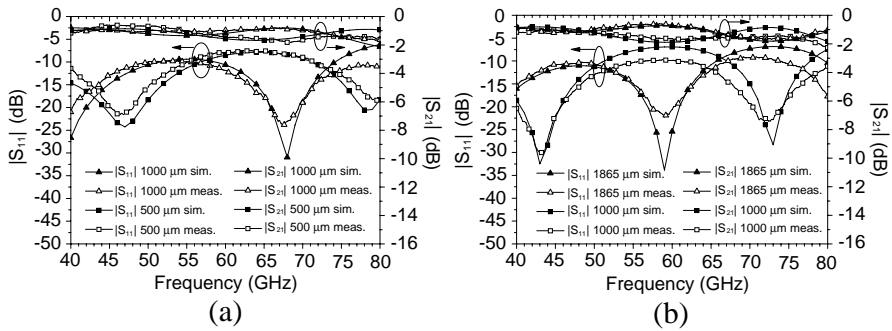


Figure 12. Measured and microwave office simulated data for (a) full membrane lines, and (b) reduced membrane lines.

Possible variations in the electrical characteristics of the GCPW line (the effects of which would have been accounted for during the TRL calibration procedure) due to variations in the slot widths were also investigated through measurement of the original photolithography masks coupled with HFSS simulations. This variation was found to be $\pm 2 \mu\text{m}$ which corresponded to a variation of around $\pm 0.5 \Omega$ in the membrane-supported stripline, $\pm 2 \Omega$ in the membrane-supported GCPW, and $\pm 3 \Omega$ in the probe-pad regions.

The values of Z_0 for in the probe-pad regions and GCPW were varied in the model along with the length-ratio of the epoxy-under-filled GCPW and membrane-supported GCPW (MS-GCPW). The loss and effective relative permittivity remained fixed in all line sections as did all the simulated parameters for the membrane-supported stripline. The results of the simulations can be seen in Figure 12(a) for 500 μm and 1000 μm full membrane lines, and Figure 12(b) for 1000 μm and 1865 μm reduced membrane lines.

In all cases a relatively good match between the measured and

modeled data implies that the HFSS simulated electrical parameters for the membrane-supported striplines studied are realistic (in the same range) when compared to the measured data obtained.

5. CONCLUSIONS

A thorough review of demonstrated state-of-the-art micromachined quasi-planar, shielded and membrane supported transmission lines for use at millimeter-wave frequencies has been given. Two new micromachined transmission lines have been proposed: a membrane-supported shielded stripline and a novel variation of this where the membrane material is removed in areas of little mechanical importance to reduce attenuation and dispersion. Membrane supported line and micromachined shielding fabrication has been outlined.

A design methodology suitable for membrane supported lines has been given along with a detailed investigation into the characteristics of the lines using rigorous FEM-based electromagnetic simulation. The simulations suggested losses as low as 0.39 dB/cm, and effective relative permittivities of about 1.044 are possible at a frequency of 100 GHz: this compares well with other demonstrated membrane supported and microshielded transmission lines at this frequency. Analysis of the single mode performance range of the lines investigated has been conducted and shown single mode performance to over 140 GHz. A detailed generalized discussion of leaky and surface wave modes on all types of membrane supported lines, whether stripline or CPW, with and without full or partial shielding has been presented.

The measurements and de-embedding techniques used have been described and the results obtained compared to simulated results. The measurement results suggest that the simulated loss characteristics of the lines are realistic, meaning performance of the transmission lines studied is comparable to previously published state-of-the-art results, but with the benefit of full shielding. The micromachining techniques demonstrated in the fabrication of the line are generally more flexible than those previously demonstrated with regards to the complexity of the structures that can be realized. This affords significant advantages in the quality and type of electromagnetic structure that can be realized using this technology, and sets the stage for the development of novel millimeter-wave components.

ACKNOWLEDGMENT

We acknowledge the support of Agilent Technologies for elements of the work that were performed when the authors were with the University of

Leeds. Roland Clarke from the Institute of Microwaves and Photonics at the University of Leeds is also thanked for help with the microwave measurements, along with Heribert Eisele for help with de-embedding the measured results.

REFERENCES

1. Chi, C.-Y. and G. M. Rebeiz, "Planar millimeter-wave microstrip lumped elements using micro-machining techniques," *IEEE Int. Microwave Theory Tech. Symposium Dig.*, 657–660, May 1994.
2. Robertson, S. V., A. R. Brown, L. P. B. Katehi, and G. M. Rebeiz, "A 10–60-GHz micromachined directional coupler," *IEEE Trans. Microwave Theory Tech.*, Vol. 46, No. 11, 1845–1849, Nov. 1998.
3. Raskin, J. P., "Micromachined W-band passive components for communication applications," *MSTnews*, 02/01, 13–15, Feb. 2001.
4. Trimmer, W. S. N., "Microrobots and micromechanical systems," *Sensors and Actuators*, Vol. 19, 267–287, 1988.
5. Rebeiz, G. M., L. P. B. Katehi, T. M. Weller, C. Y. Chi, and S. V. Robertson, "Micromachined membrane filters for microwave and millimetre-wave applications (Invited article)," *Int. J. of Microwave and Millimeter-wave Computer Aided Engineering*, Vol. 7, 149–166, Feb. 1997.
6. Petersen, K. E., "Silicon as a mechanical material," *Proc. IEEE*, Vol. 70, No. 5, 420–457, May 1982.
7. Moore, D. F. and R. R. A. Syms, "Recent developments in micromachined silicon," *Electronics and Communication Engineering Journal*, Vol. 11, No. 6, 261–270, Dec. 1999.
8. Mehregany, M., "Microelectromechanical systems," *IEEE Circuits and Devices*, Vol. 9, 14–22, Jul. 1993.
9. Rebeiz, G. M., *RF MEMS: Theory, Design and Technology*, John Wiley and Sons, 2003.
10. Herrick, K. J., T. A. Schwarz, and L. P. B. Katehi, "Si-micromachined coplanar waveguides for use in high-frequency circuits," *IEEE Trans. Microwave Theory Tech.*, Vol. 46, No. 6, 762–768, Jun. 1998.
11. Newlin, D. P., A.-V. H. Pham, and J. E. Harriss, "Development of low loss organic micromachined interconnects on silicon at microwave frequencies," *IEEE Trans. On Components and Packaging Technologies*, Vol. 25, No. 3, 506–510, Sep. 2002.
12. Drayton, R. F. and L. P. B. Katehi, "Development of self-packaged high frequency circuits using micromachining techniques," *IEEE*.

- Trans. Microwave Theory Tech.*, Vol. 41, No. 9, 2073–2080, Sep. 1995.
13. Park, J. Y., C. W. Baek, S. Jung, H. T. Kim, Y. Kwon, and Y. K. Kim, “Novel micromachined coplanar waveguide transmission lines for applications in millimetre-wave circuits,” *Journal of Applied Physics*, Vol. 39, 7120–7124, 2000.
 14. Herrick, K. J., T. A. Schwarz, and L. P. B. Katehi, “Si-micromachined coplanar waveguides for use in high-frequency circuits,” *IEEE Trans. Microwave Theory Tech.*, Vol. 46, No. 6, 762–768, Jun. 1998.
 15. Ponchak, G. E., A. Margomenos, and L. P. B. Katehi, “Low-loss CPW on low-resistivity Si substrates with a micromachined polyimide interface layer for RFIC interconnections,” *IEEE Trans. Microwave Theory Tech.*, Vol. 49, No. 5, 866–870, 2001.
 16. Newlin, D. P., A.-V. H. Pham, and J. E. Harris, “Development of low loss organic-micromachined interconnects on silicon at microwave frequencies,” *IEEE Trans. Components and Packaging Technologies*, Vol. 25, No. 3, 506–510, Sep. 2002.
 17. Weller, T. M., L. P. Katehi, and G. M. Rebeiz, “High performance microshield line components,” *IEEE Trans. Microwave Theory Tech.*, Vol. 43, No. 3, 534–543, Mar. 1995.
 18. Lee, K. Y., N. LaBianca, S. A. Rishton, S. Zolgharnain, J. D. Gelorme, J. Shaw, and T. H. P. Chang, “Micromachining applications of a high resolution ultrathick photoresist,” *J. Vacuum Science and Technology B.*, Vol. 13, No. 6, 3012–3016, Nov./Dec. 1995.
 19. Lorenz, H., M. Despont, N. Fahrni, N. LaBianca, P. Renaud, and P. Vettiger, “SU-8: A low-cost negative resist for MEMS,” *J. of Micromechanical Microengineering*, Vol. 7, 121–124, 1997.
 20. Despont, M., H. Lorenz, N. Fahrni, J. Brugger, P. Renaud, and P. Vettiger, “High-aspect-ratio, ultrathick, negative-tone near-UV photoresist for MEMS applications,” *IEEE Proc. Int. Workshop on Micro-Electro Mechanical Systems*, 518–522, Jan. 1997.
 21. Lorenz, H., M. Laudon, and P. Renaud, “Mechanical characterization of a new high-aspect-ratio near UV-photoresist,” *J. Micro-electronic Engineering*, Vol. 41/42, 371–374, 1998.
 22. Farrington, N. E. S., “Micromachined transmission line interconnects for millimetre-wave multi-chip modules,” Ph.D. Thesis, School of Electrical and Electronic Engineering, the University of Leeds, 2005.
 23. Shu, Y., X. Qi, and Y. Wang, “Analysis equation for

- shielded suspended substrate microstrip line and broadside-coupled stripline,” *IEEE Int. Microwave Theory Tech. Symposium Dig.*, 693–696, 1987.
24. High Frequency Structure Simulator (HFSS) Version 12, Ansoft, Pittsburgh, PA, USA.
 25. Rizzi, P. A., *Microwave Engineering — Passive Circuits*, Prentice Hall International Inc., 1988.
 26. Shigesawa, H., M. Tsuji, and A. A. Oliner, “Simultaneous propagation of bound and leaky dominant modes on printed circuit lines: A new general effect,” *IEEE Trans. Microwave Theory Tech.*, Vol. 43, No. 12, 3007–3019, Dec. 1995.
 27. Tsuji, M., H. Shigesawa, and A. A. Oliner, “New interesting leakage behaviour on coplanar waveguides of finite and infinite widths,” *IEEE Trans. Microwave Theory Tech.*, Vol. 39, No. 12, 2130–2137, Dec. 1991.
 28. Oliner, A. A., “Leaky waves: Basic properties and applications,” *Asia-Pacific Microwave Conference Proc., APMC’97*, Vol. 1, 397–400, Dec. 1997.
 29. Mesa, F. and R. Marquis, “Low frequency leaky regime in covered multilayered structures,” *IEEE Trans. Microwave Theory Tech.*, Vol. 44, No. 9, 1521–1525, Sep. 1996.
 30. Nghiem, D., J. T. Williams, D. R. Jackson, and A. A. Oliner, “Leakage of the dominant mode on stripline with a small air gap,” *IEEE Trans. Microwave Theory Tech.*, Vol. 43, No. 11, 2549–2556, Nov. 1995.
 31. Yaozhong, L., C. Kimin, and T. Itoh, “Non-leaky coplanar (NLC) waveguides with conductor backing,” *IEEE Trans. Microwave Theory Tech.*, Vol. 43, No. 5, 1067–1072, May 1995.
 32. Mesa, F., A. A. Oliner, D. R. Jackson, and M. J. Freire, “The influence of a top cover on the leakage from microstrip line,” *IEEE Trans. Microwave Theory Tech.*, Vol. 48, No. 12, 2240–2248, Dec. 2000.
 33. Nghiem, D., J. T. Williams, D. R. Jackson, and A. A. Oliner, “Suppression of leakage on stripline and microstrip structures,” *IEEE Int. Microwave Theory Tech. Symposium Dig.*, Vol. 1, 145–148, May 1994.
 34. Collin, R. E., *Field Theory of Guided Waves*, McGraw-Hill, 1960.
 35. Godshalk, E. M., “Generation and observation of surface waves on dielectric slabs and coplanar structures,” *IEEE Int. Microwave Theory Tech. Symposium Dig.*, 923–925, 1993.
 36. Dib, N. I., W. P. Harokopus, Jr., P. B. Katehi, C. C. Ling, and

- G. M. Rebeiz, "Study of a novel planar transmission line," *IEEE Int. Microwave Theory Tech. Symposium Dig.*, 623–626, 1991.
37. Weller, T. M., G. M. Rebeiz, and L. P. Katehi, "Experimental results on microshield transmission line circuits," *IEEE Int. Microwave Theory Tech. Symposium Dig.*, 827–830, 1993.
 38. Cheng, H., J. F. Whitaker, T. M. Weller, and L. P. B. Katehi, "Terahertz-bandwidth characterisation of coplanar waveguide via time domain electro-optic sampling," *IEEE Int. Microwave Theory Tech. Symposium Dig.*, 477–480, 1994.
 39. Duwe, K., S. Hirsch, R. Judaschke, and J. Muller, "Micromachined coplanar waveguides on thin HMDSN-membranes," *25th Int. Conference on Infrared and Millimeter Waves Digest*, 297–298, Sep. 2000.
 40. Liu, W. Y., D. P. Steenson, and M. B. Steer, "Membrane-supported CPW with mounted active devices," *IEEE Microwave and Wireless Components Letters*, Vol. 11, No. 4, 167–169, Apr. 2001.
 41. Advanced Wave Research Corporation, Microwave Office, 1960 E. Grand Avenue, Suite 430, CA 90245.